Electronic Supplementary Material (ESI) for Physical Chemistry Chemical Physics.

Supporting Information

One-Bond ^{13}C-^{13}C Spin-Coupling Constants in Saccharides: A Comparison of Experimental and Calculated Values By Density Functional Theory Using Solid-State ^{13}C NMR and X-Ray Crystallography

Timothy Tetrault,[1] Reagan J. Meredith,[1] Mi-Kyung Yoon,[1,4] Christopher Canizares,[1] Allen G. Oliver,[2] Ian Carmichael,[3] and Anthony S. Serianni[1*]

[1]Department of Chemistry and Biochemistry, [2]Molecular Structure Facility, and [3]Radiation Laboratory, University of Notre Dame, Notre Dame, IN 46556-5670 USA; [4]Omicron Biochemicals, Inc., South Bend, IN 46617 USA

*Corresponding author: aseriann@nd.edu

Table of Contents

Synthesis of ^{13}C-Labeled Compounds 1–5

Starting materials and reagents were commercial grade and were used without further purification. ^{13}C-Labeled D-aldohexoses were obtained from Omicron Biochemicals, Inc. (South Bend, IN) and used without further purification. All reactions were monitored by thin-layer

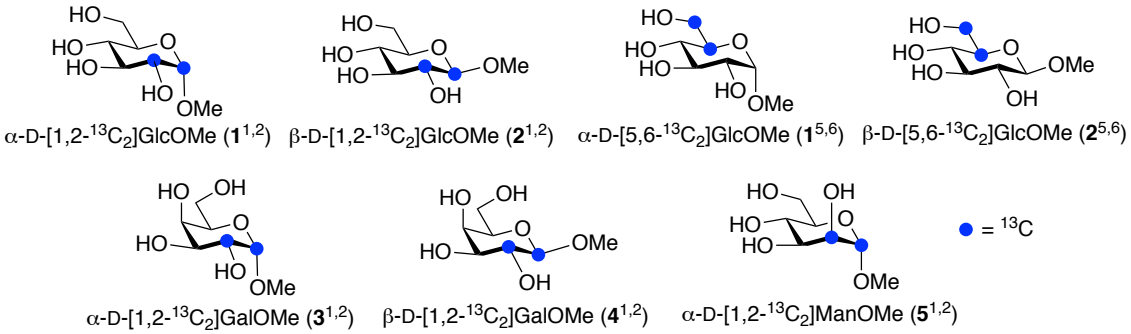

Scheme S1. Chemical structures of the selectively ^{13}C-labeled monosaccharides **1**^{1,2}, **2**^{1,2}, **3**^{1,2}, **4**^{1,2}, **5**^{1,2}, **1**^{5,6} and **2**^{5,6} used in this study. $^{1}J_{C1,C2}$ was measured in the five compounds ^{13}C-labeled at both C1 and C2, and $^{1}J_{C5,C6}$ was measured in the two compounds ^{13}C-labeled at C5 and C6.

chromatography (TLC) on aluminum sheets coated with Silica Gel 60 (F_{254}, 250 μm thickness). Spots were detected with a cerium molybdate stain.[1] Column chromatography was conducted using Dowex 1 x 8 (200–400 mesh) anion-exchange resin (200–400 mesh) in the OH^- form.[2] High-resolution mass spectrometry (HRMS) data were obtained on a Bruker micrOTOF-QII quadrupole time-of-flight (QTOF) mass spectrometer operating in the ESI mode.

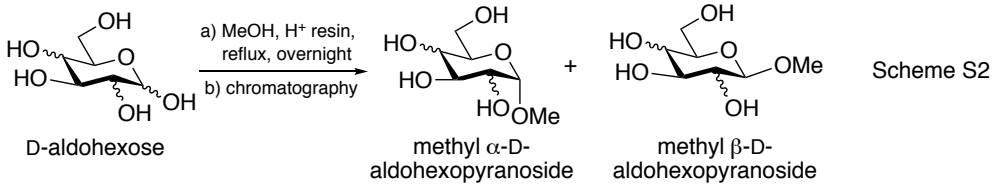

Scheme S2

*1.1. General Procedure To Prepare ^{13}C-labeled **1–5** (Schemes S1 and S2).* Dowex 50 x 8 (200-400 mesh) cation-exchange resin in the H^+ form (250 mg; dried at >100 °C under high vacuum for 2 h), the ^{13}C-labeled D-aldohexose (250 mg, 1.39 mmol) was added to MeOH (10 mL), and the mixture was refluxed overnight with stirring. After cooling to RT, the resin was removed by filtration and the filtrate was concentrated at 30° *in vacuo*. The crude residue was dissolved in a minimal volume of distilled water, and the solution was applied to a chromatography column (2.5 cm x 100 cm) containing Dowex 1 x 8 (200–400 mesh) anion-exchange resin in the OH^- form.[2] The column was eluted with decarbonated, distilled water and fractions (10 mL) were assayed by TLC analysis using a cerium molybdate stain[1] and charring with a heat gun. For **1–4** (Glc and Gal), the α-anomer eluted first, followed by the β-anomer. For **5** (Man), the β-anomer eluted first, followed by the α-anomer. Yields: **1**^{1,2}, 45.6% as a white solid; **2**^{1,2}, 22.4% as a white solid; **1**^{5,6}, 46.3% as a white solid; **2**^{5,6}, 29.4% as a white solid; **3**^{1,2}, 43.0% as a white solid; **4**^{1,2},

17.6% as a white solid; **5**[1,2], 60.3% as a flaky white solid. ^{1}H and $^{13}C\{^{1}H\}$ NMR spectra of isolated products matched those in the literature,[3–7] except for the additional line-splitting from J_{CH} to the ^{13}C-labeled carbons (^{1}H spectra), and relative line intensities (strong signals from the ^{13}C-labeled carbons) and additional line-splitting from J_{CC} to the ^{13}C-labeled carbons (^{13}C spectra) .

For ^{13}C-labeled D-mannose: 100 mg (0.56 mmol), H^+ resin (100 mg), MeOH (5 mL).

High-Resolution Mass Spectrometry (HRMS) Data for Compounds **1**–**5**

m/z	**compound**						
	1[1,2]	**1**[5,6]	**2**[1,2]	**2**[5,6]	**3**[1,2]	**4**[1,2]	**5**[1,2]
Calculated, $[M+Na]^+$	219.074969	219.074969	219.074969	219.074969	219.0750	219.0750	219.074969
Found, $[M+Na]^+$	219.075543	219.074921	219.077388	219.075842	219.0742	219.0743	219.073698

Crystallization and X-ray Crystallography of 1–5

All compounds (**1**^{1,2}, **1**^{5,6}, **2**^{1,2}, **2**^{5,6}, **3**^{1,2}, **4**^{1,2}, **5**^{1,2}) were dissolved in a concentrated solution of ~95:5 *v*/*v* methanol:water with heat and crystallized at RT by slow evaporation. Crystal structures were determined at 120 K (–173 °C) with monochromated copper Kα radiation to a resolution of 0.8 Å. All atoms were refined freely including hydrogen. The final structures were virtually identical to those reported previously;[4,8–15] the presence of ^{13}C atoms did not alter the structures to any appreciable extent.

The structures gave the following torsion angles involving hydroxyl hydrogens:

1^{1,2} (tt2101):	C1–C2–O2–H (θ_2)	–77.1(19)	[–77.1 ± 5.7]
1^{5,6} (tt2202):	C1–C2–O2–H (θ_2)	–77.2(18)	[–77.2 ± 5.4]
1^{5,6} (tt2202):	C5–C6–O6–H (θ_6)	–88.3(19)	[–88.3 ± 5.7]
2^{1,2} (tt2203):	C1–C2–O2–H (θ_2)	92.0(16)	[92.0 ± 4.8]
2^{5,6} (tt2104):	C1–C2–O2–H (θ_2)	92.2(17)	[92.2 ± 5.1]
2^{5,6} (tt2104):	C5–C6–O6–H (θ_6)	–57.9(16)	[–57.9 ± 4.8]
3^{1,2} (tt2102):	C1–C2–O2–H (θ_2)	123.0(17)	123.0 ± 5.1]
4^{1,2} (tt2103):	C1–C2–O2–H (θ_2)	97.7(18)	[97.7 ± 5.4]
5^{1,2} (tt2201):	C1–C2–O2–H (θ_2)	170.0(17)	[170.0 ± 5.1]

The values in parentheses are standard uncertainties (SU) of the average torsion angle. The values in brackets are the average torsion angle with range calculated as 3 x SU (99% confidence interval). Cartesian coordinates for the seven structures were deposited in the Cambridge Structural Database and can be accessed using the following deposition numbers:

1^{1,2}: Deposition Number 2252830
1^{5,6}: Deposition Number 2252831
2^{1,2}: Deposition Number 2252833
2^{5,6}: Deposition Number 2252828
3^{1,2}: Deposition Number 2252829
4^{1,2}: Deposition Number 2252827
5^{1,2}: Deposition Number 2252832

Solution ^{1}H and $^{13}C\{^{1}H\}$ NMR Spectra of $\mathbf{1}^{1,2}$–$\mathbf{5}^{1,2}$, $\mathbf{1}^{5,6}$ and $\mathbf{2}^{5,6}$

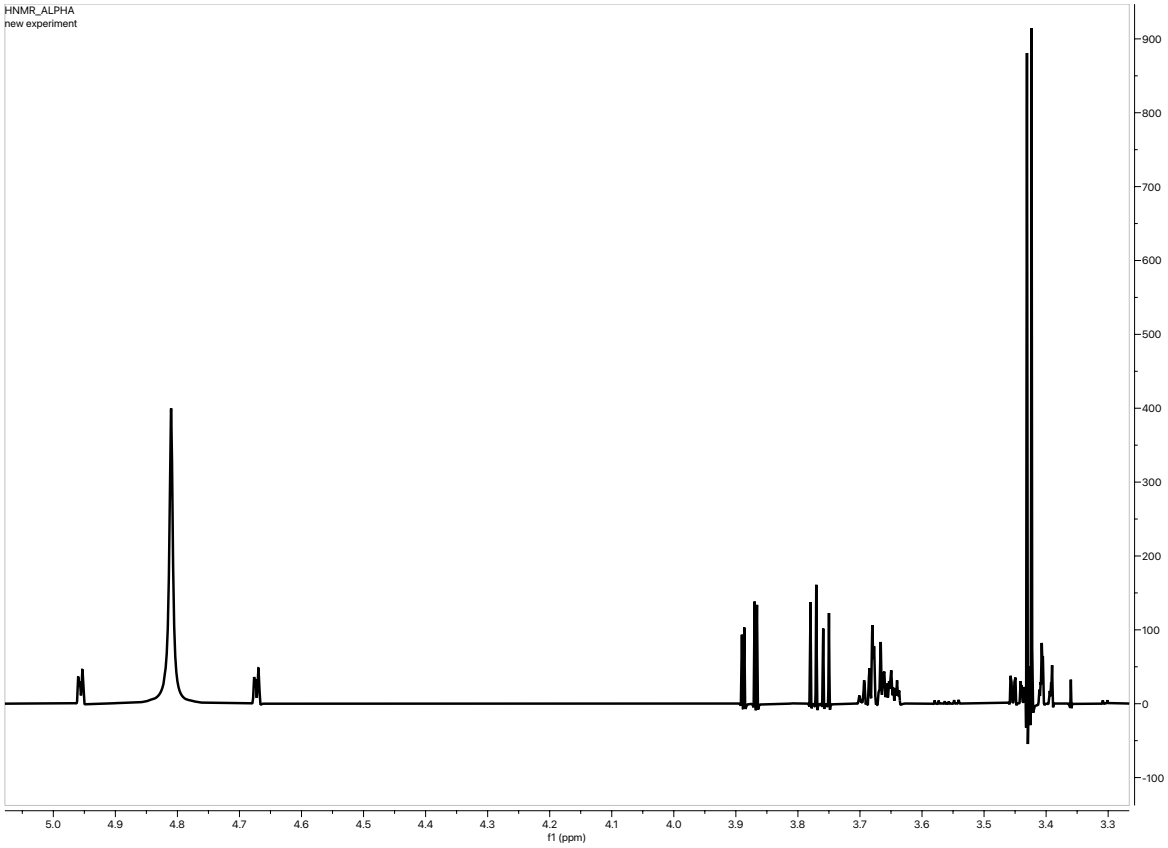

^{1}H NMR spectrum of methyl α-D-[1,2-$^{13}C_2$]glucopyranoside ($\mathbf{1}^{1,2}$)

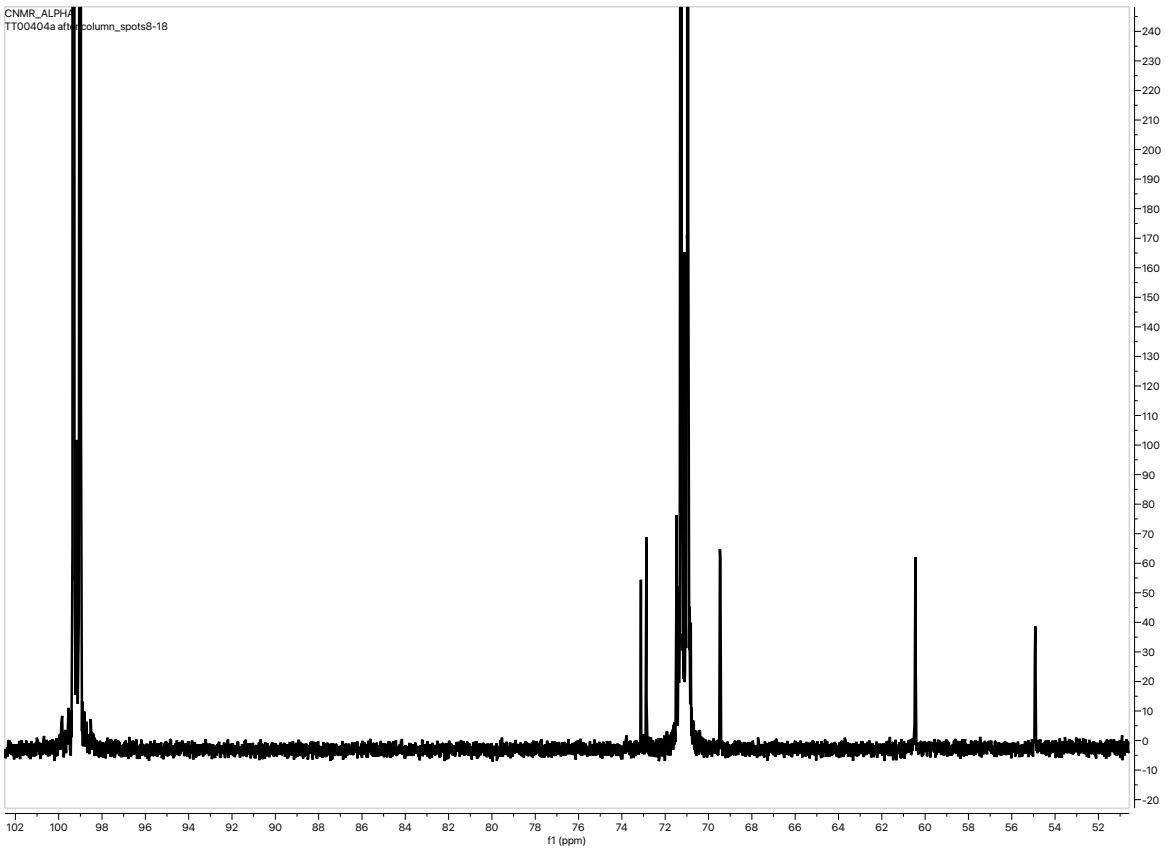

$^{13}C\{^{1}H\}$ NMR spectrum of methyl α-D-[1,2-$^{13}C_2$]glucopyranoside (**1**^{1,2})

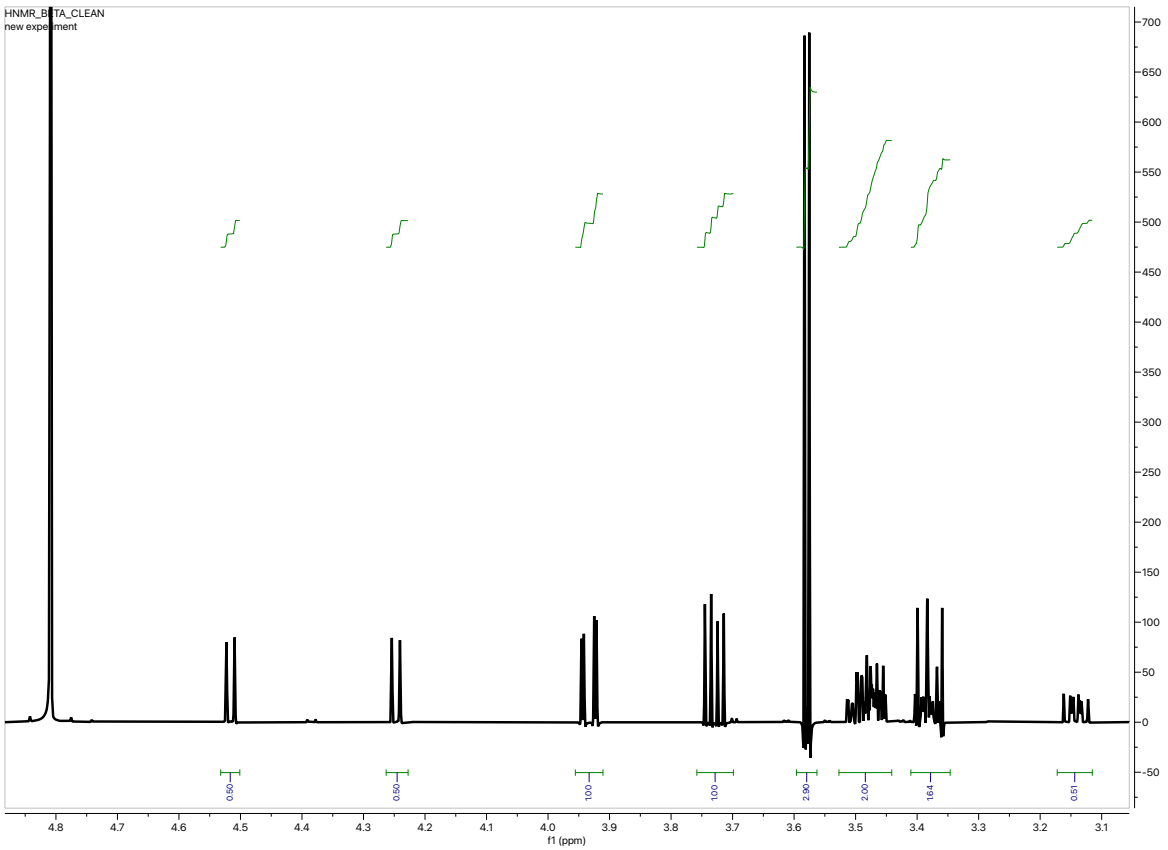

^{1}H NMR spectrum of methyl β-D-[1,2-$^{13}C_2$]glucopyranoside (**2**^{1,2})

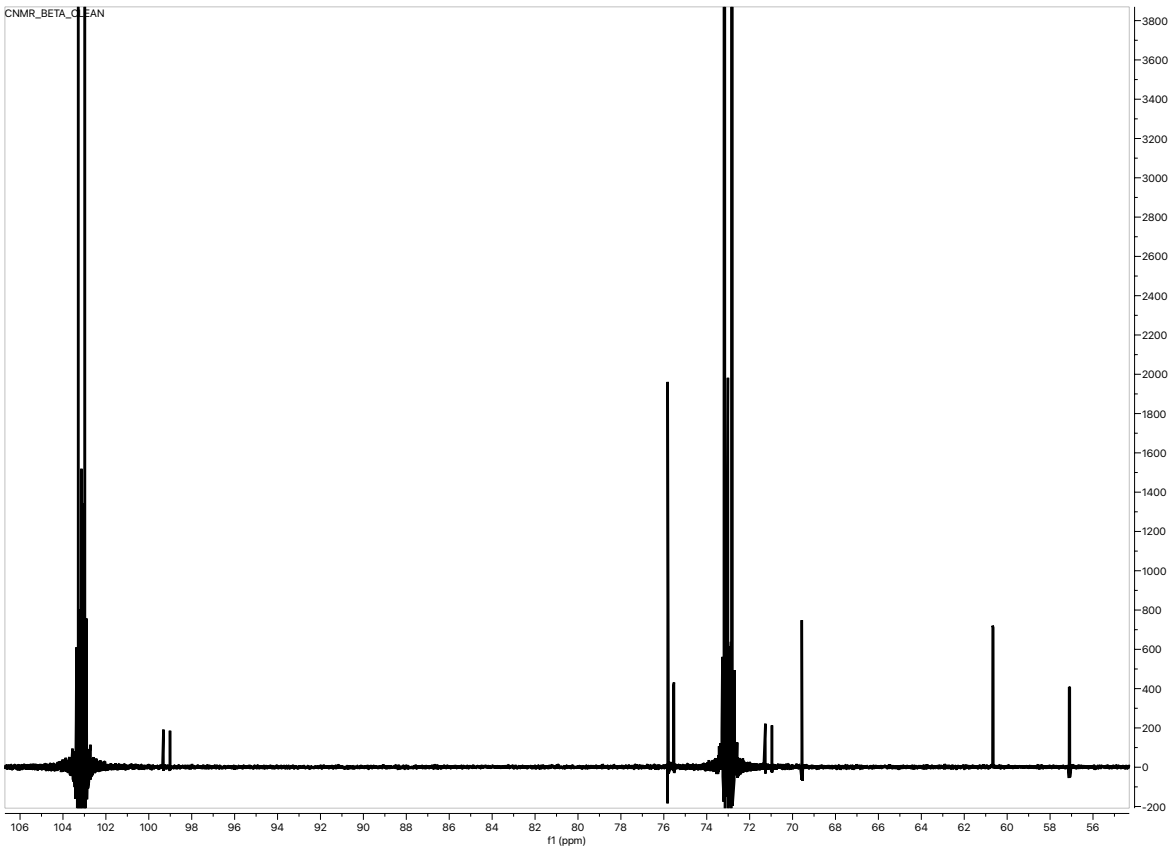

$^{13}C\{^{1}H\}$ NMR spectrum of methyl β-D-[1,2-$^{13}C_2$]glucopyranoside (**2**^{1,2})

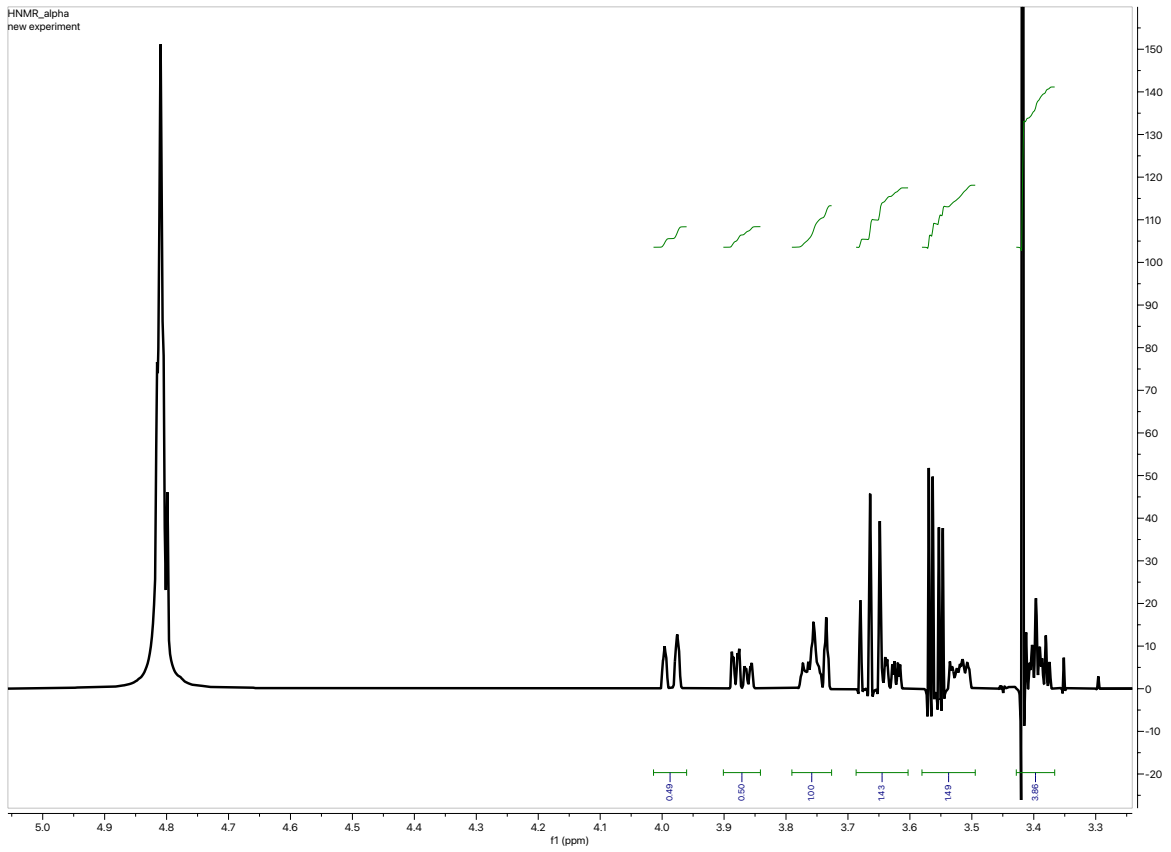

^{1}H NMR spectrum of methyl α-D-[5,6-$^{13}C_2$]glucopyranoside (**1**^{5,6})

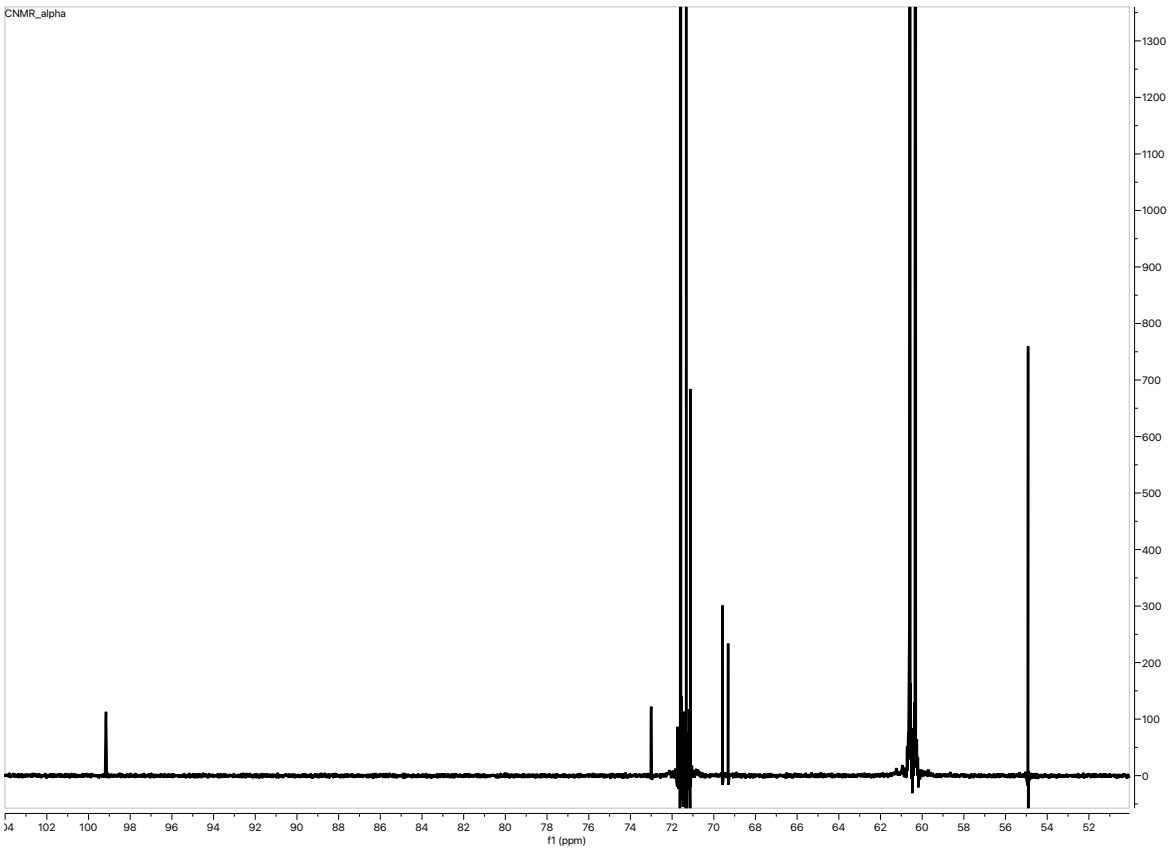

$^{13}C\{^{1}H\}$ NMR spectrum of methyl α-D-[5,6-$^{13}C_2$]glucopyranoside (**1**^{5,6})

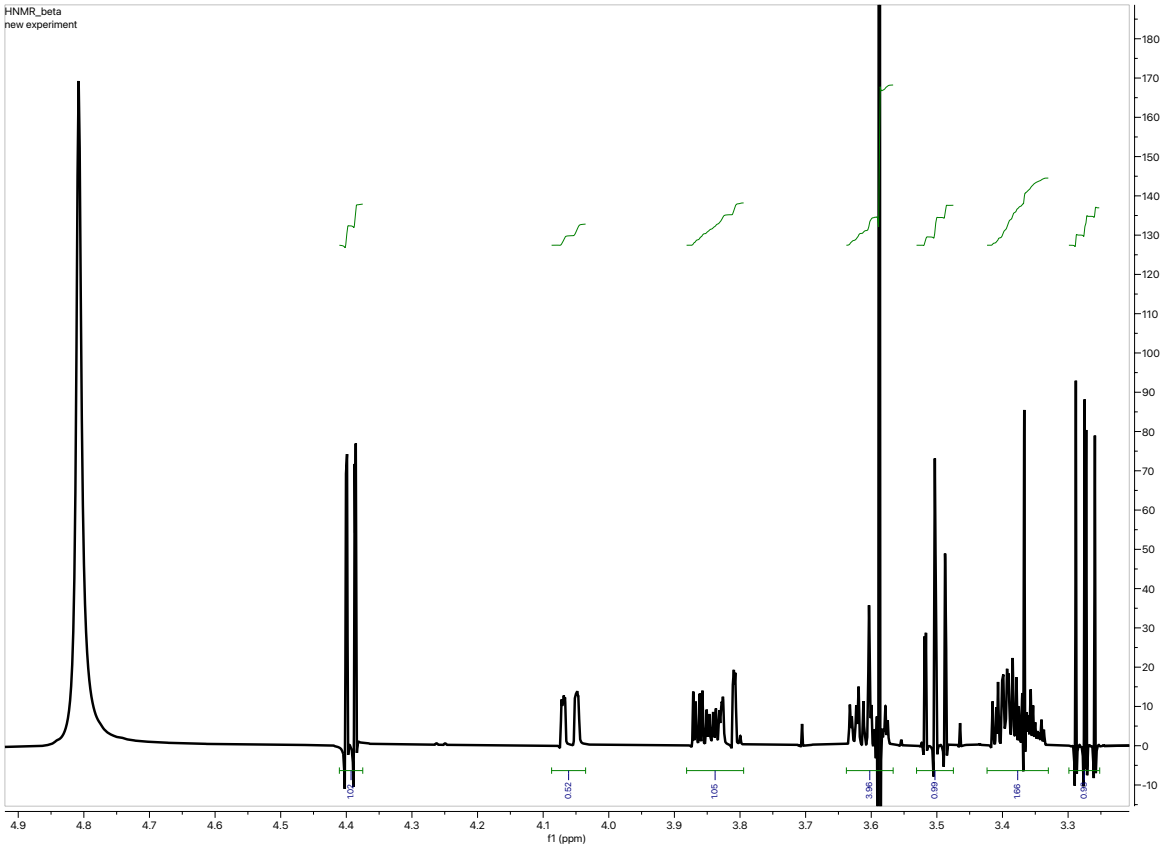

^{1}H NMR spectrum of methyl β-D-[5,6-$^{13}C_2$]glucopyranoside (**2**^{5,6})

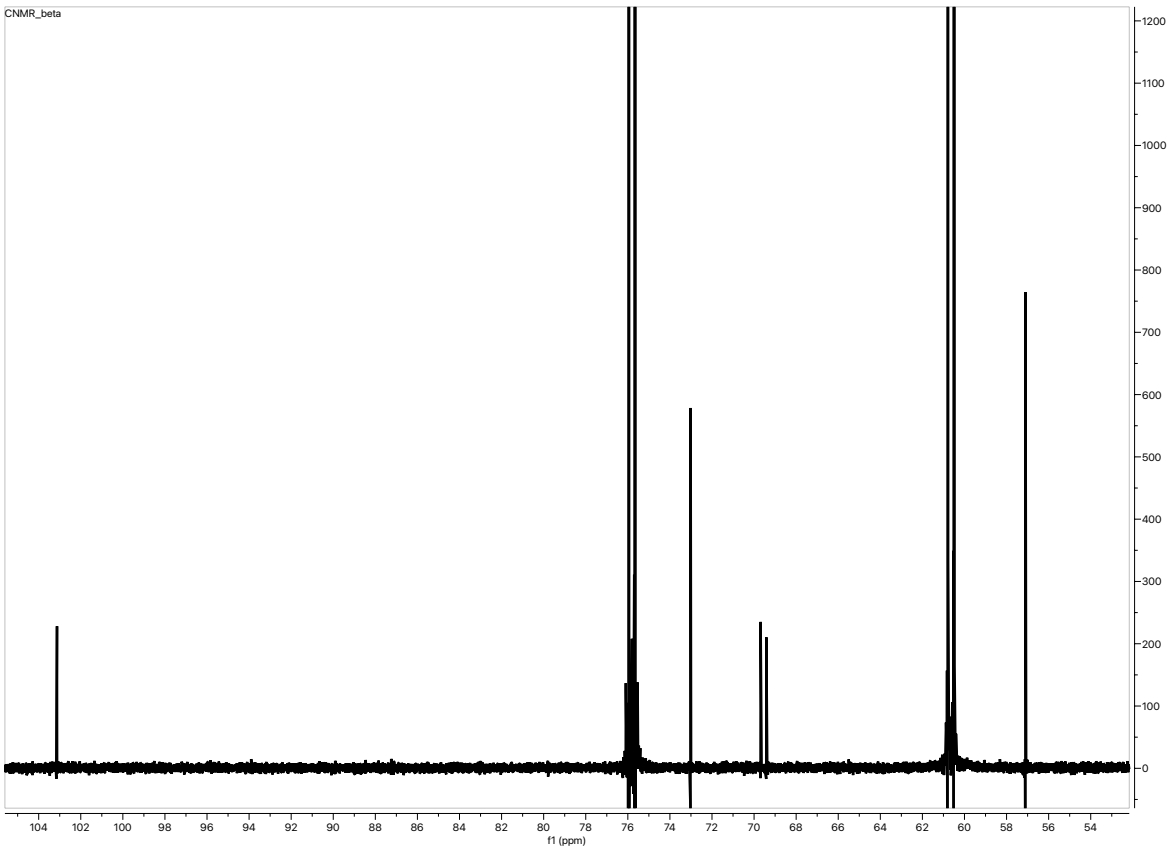

$^{13}C\{^{1}H\}$ NMR spectrum of methyl β-D-[5,6-$^{13}C_2$]glucopyranoside (**2**^{5,6})

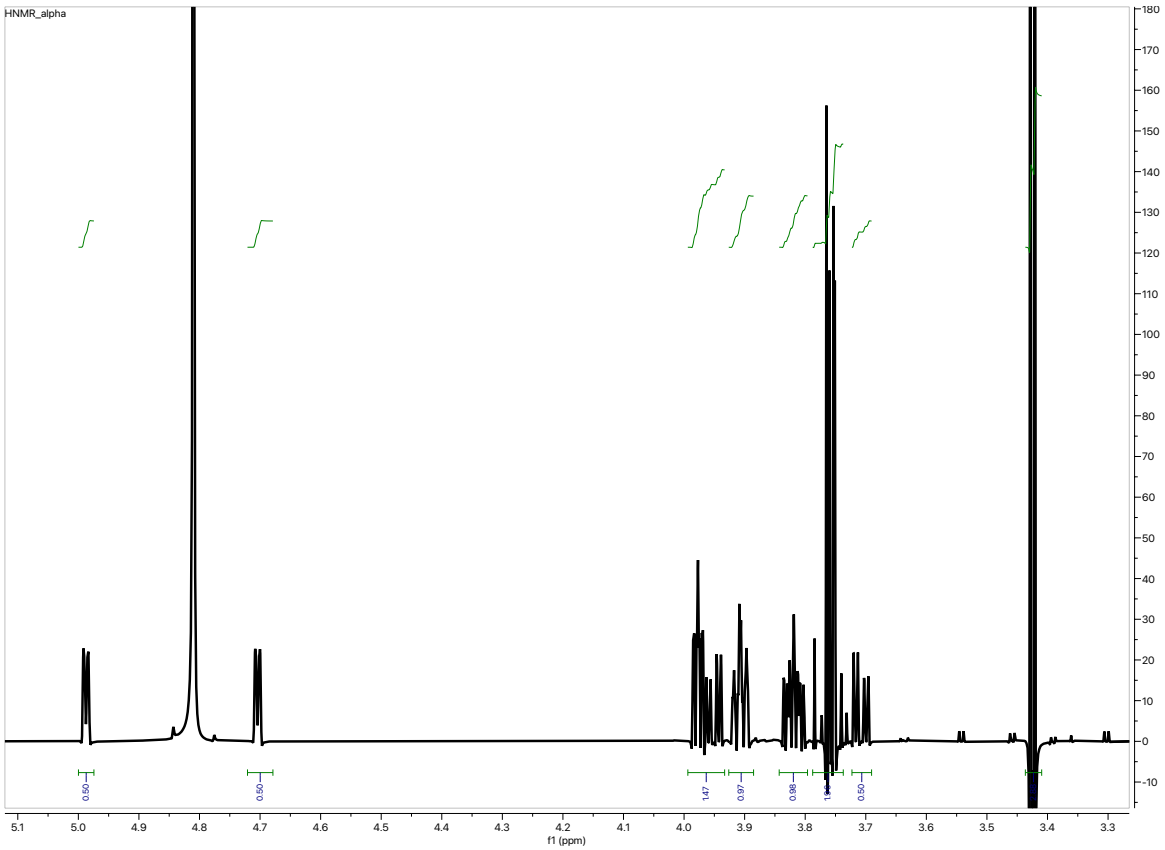

^{1}H NMR spectrum of methyl α-D-[1,2-$^{13}C_2$]galactopyranoside (**3**^{1,2})

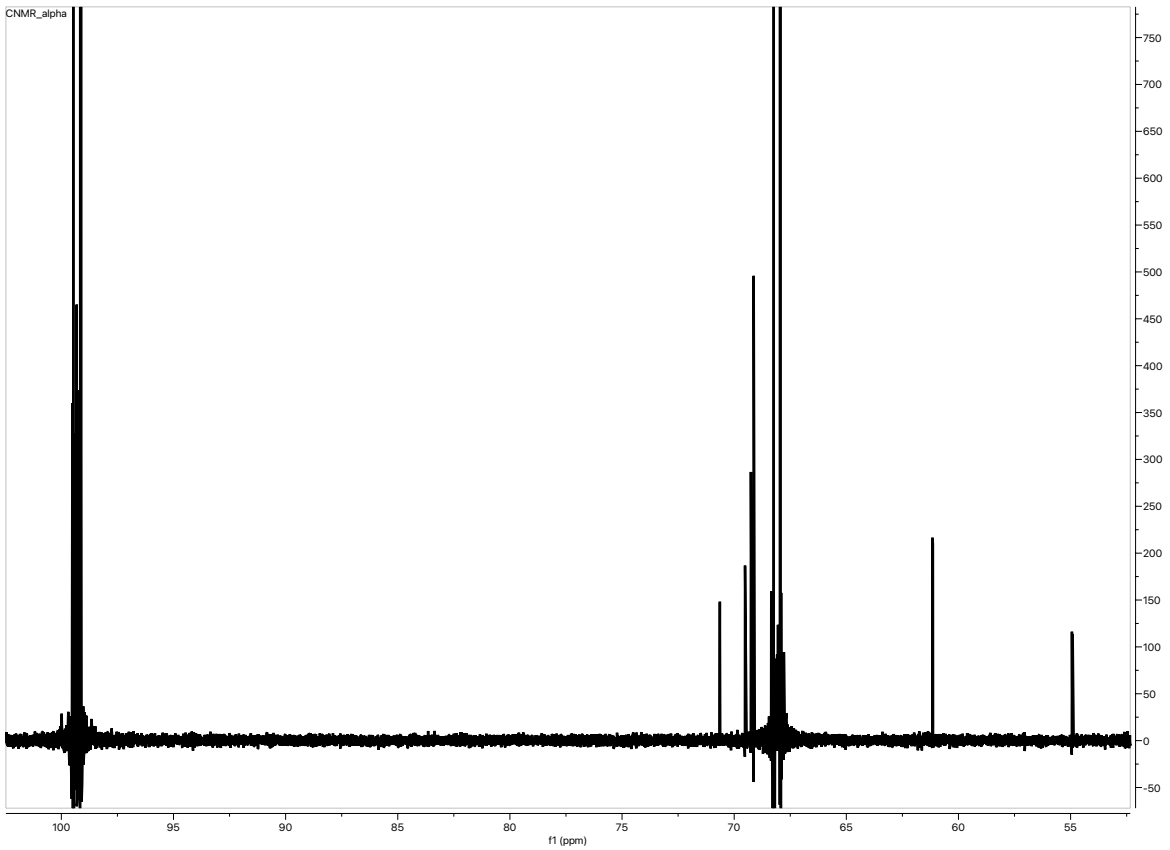

$^{13}C\{^{1}H\}$ NMR spectrum of methyl α-D-[1,2-$^{13}C_2$]galactopyranoside (**3**^{1,2})

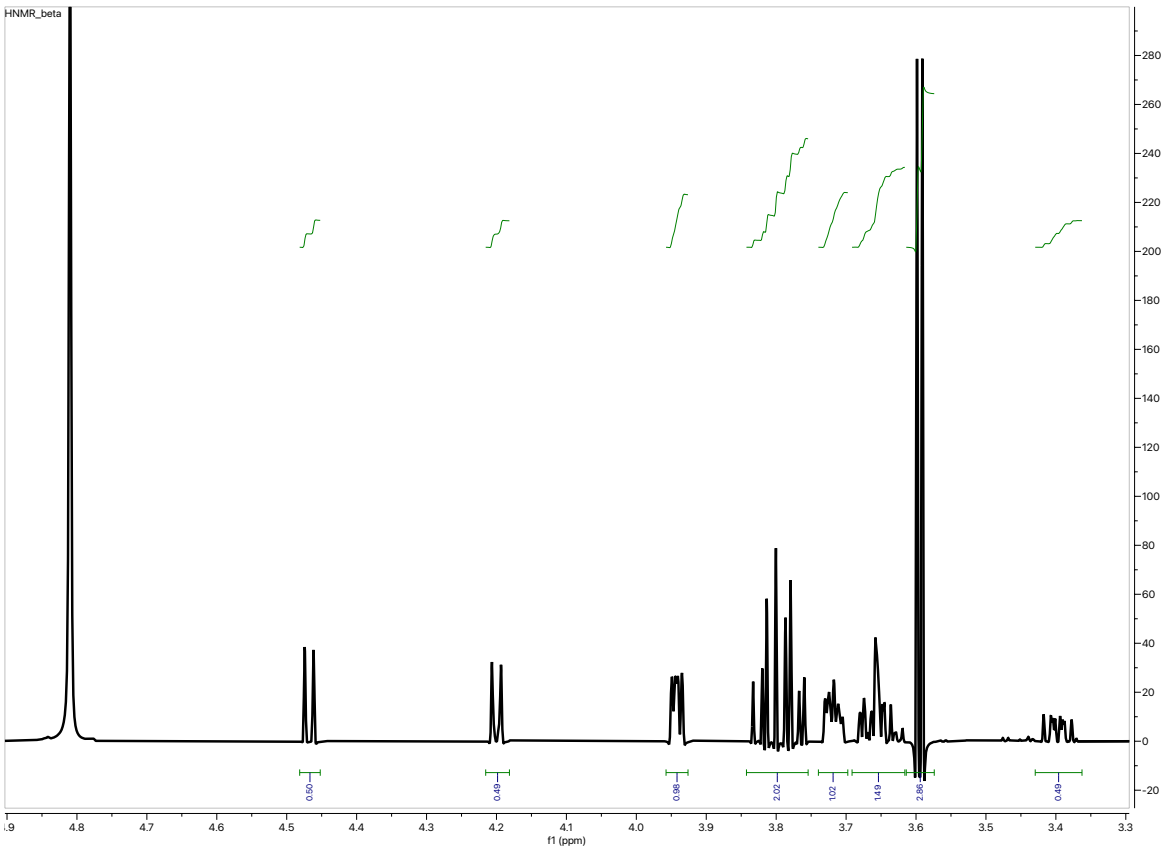

^{1}H NMR spectrum of methyl β-D-[1,2-$^{13}C_2$]galactopyranoside (**4**^{1,2})

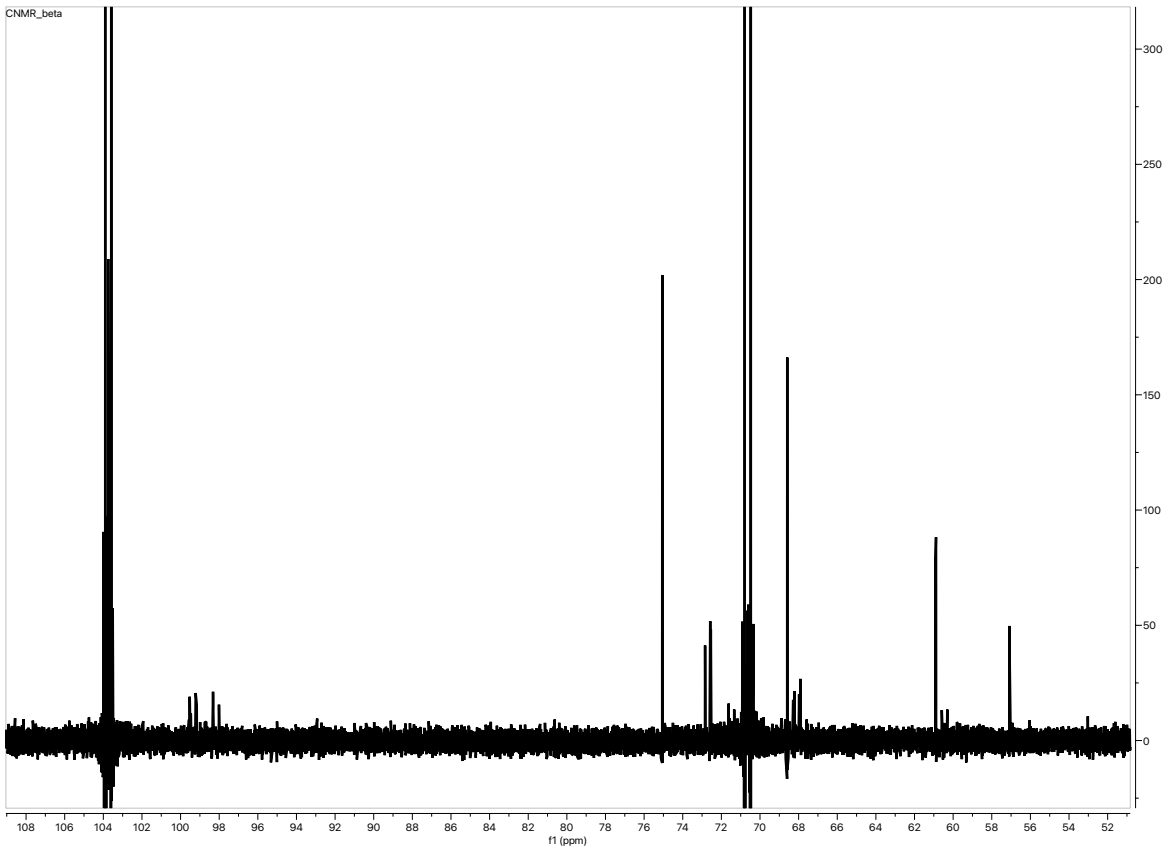

$^{13}C\{^{1}H\}$ NMR spectrum of methyl β-D-[1,2-$^{13}C_2$]galactopyranoside (**4**^{1,2})

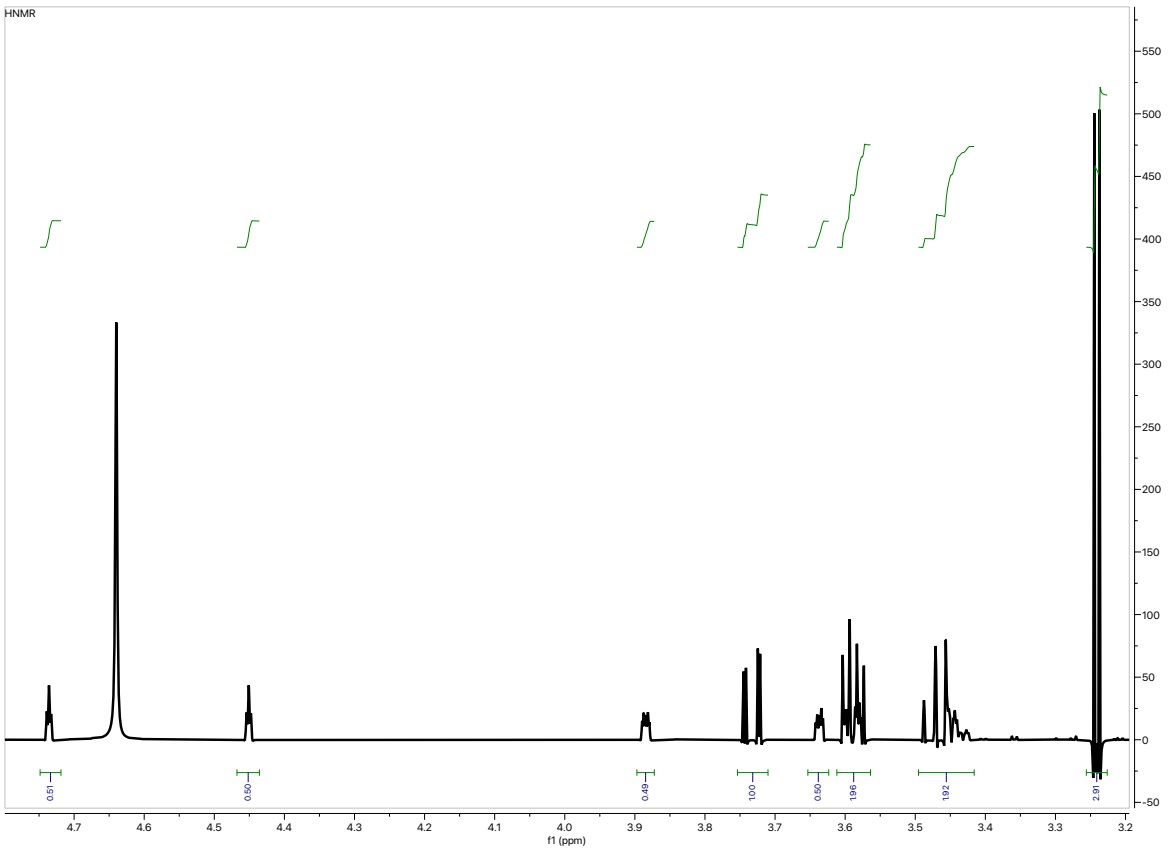

^{1}H NMR spectrum of methyl α-D-[1,2-$^{13}C_2$]mannopyranoside (**5**^{1,2})

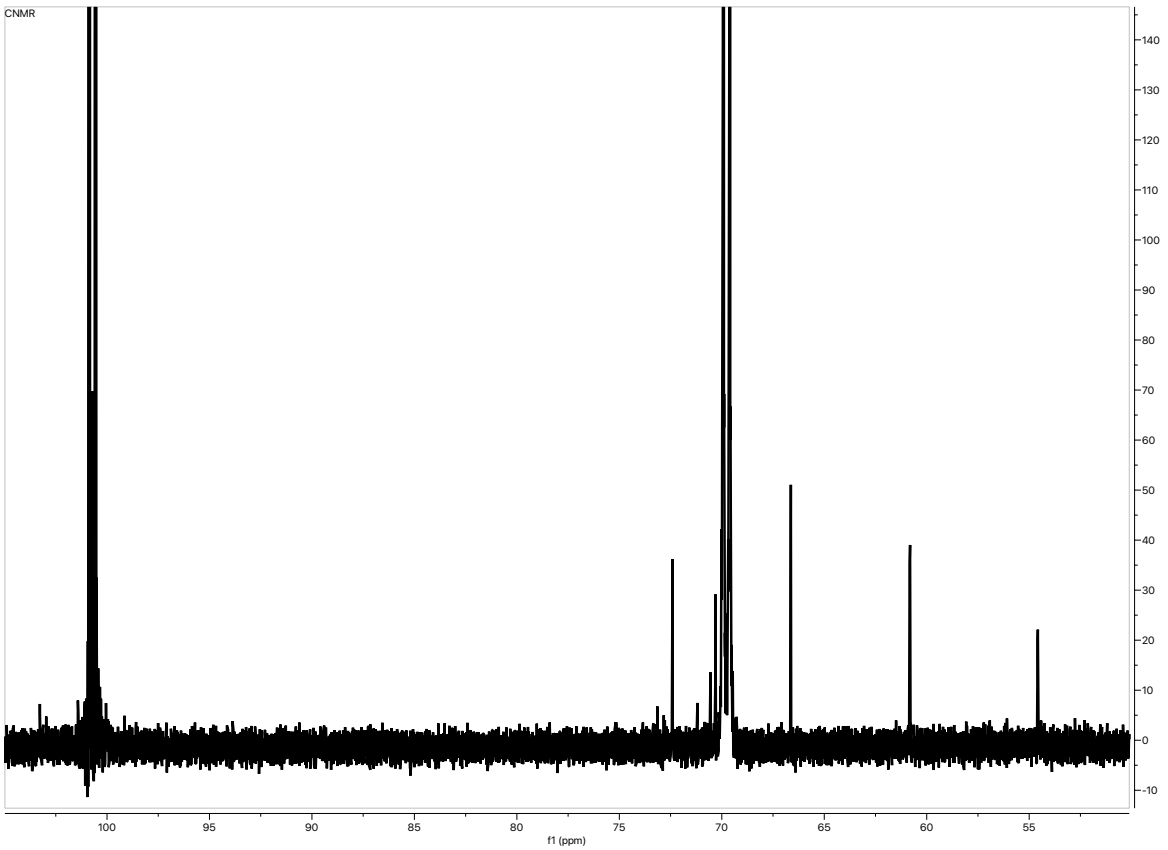

$^{13}C\{^{1}H\}$ NMR spectrum of methyl α-D-[1,2-$^{13}C_2$]mannopyranoside (**5**^{1,2})

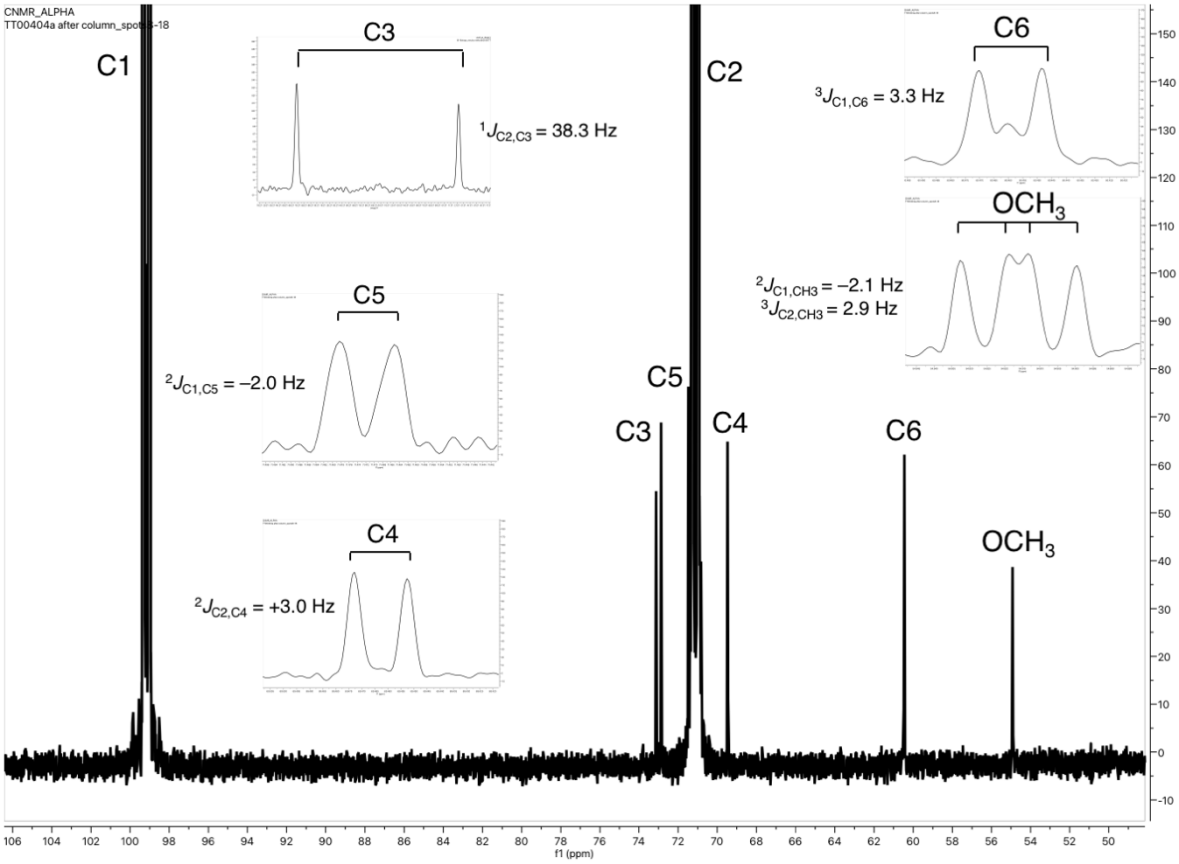

Figure S1. Partial $^{13}C[^{1}H\}$ NMR spectrum of **1**[1,2], showing the natural abundance carbons. Insets are expanded signals from C3, C4, C5, C6 and OCH_3 showing their multiplicities due to ^{13}C-^{13}C spin-coupling to the labeled carbons and the assigned J_{CC} values. Signs of the $^{2}J_{CC}$ values were taken from references 16 and 17.

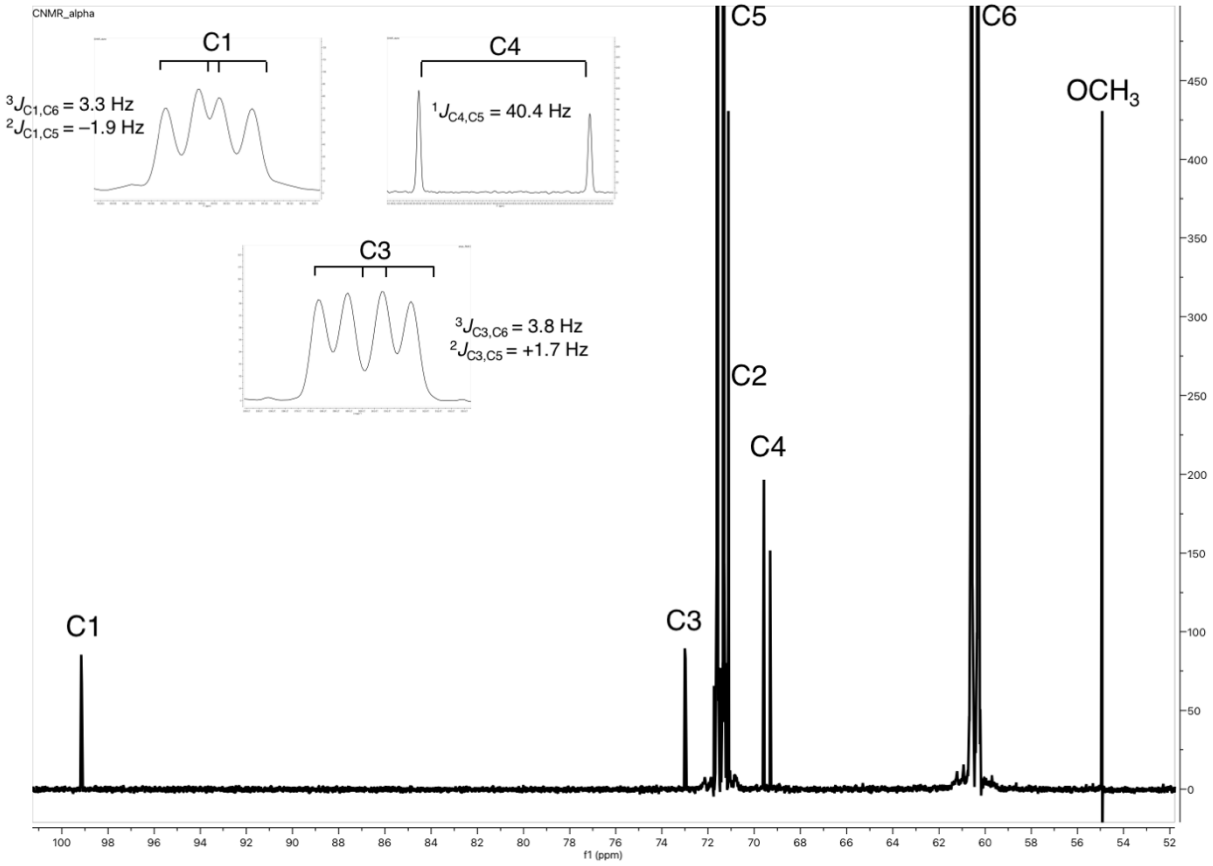

Figure S2. Partial $^{13}C[^1H\}$ NMR spectrum of **1**[5,6], showing the natural abundance carbons. Insets are expanded signals from C3, C4, and C5 showing their multiplicities due to ^{13}C-^{13}C spin-coupling to the labeled carbons and the assigned J_{CC} values. Signs of the $^2J_{CC}$ were taken from references 16 and 17. The OCH_3 signal was a sharp singlet, and the C2 signal (not shown) was a slightly broadened singlet.

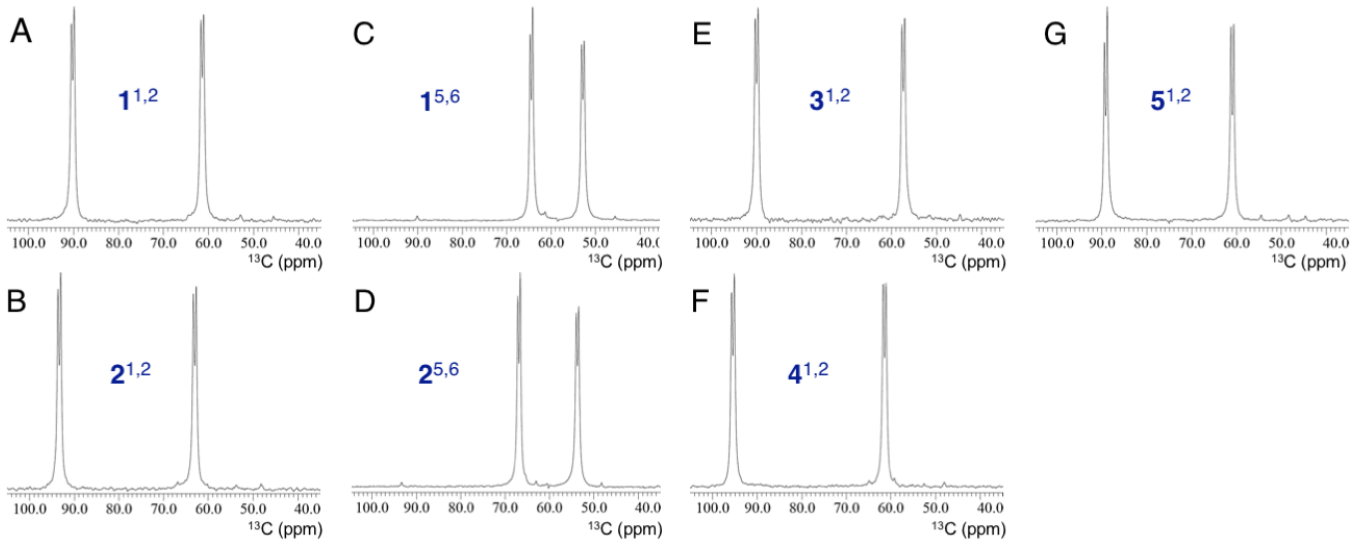

Figure S3. Solid-state ^{13}C NMR spectra of $\mathbf{1}^{1,2}$ (A), $\mathbf{2}^{1,2}$ (B), $\mathbf{1}^{5,6}$ (C), $\mathbf{2}^{5,6}$ (D), $\mathbf{3}^{1,2}$ (E), $\mathbf{4}^{1,2}$ (F) and $\mathbf{5}^{1,2}$ (G) showing only the signals from the two ^{13}C-labeled carbons.

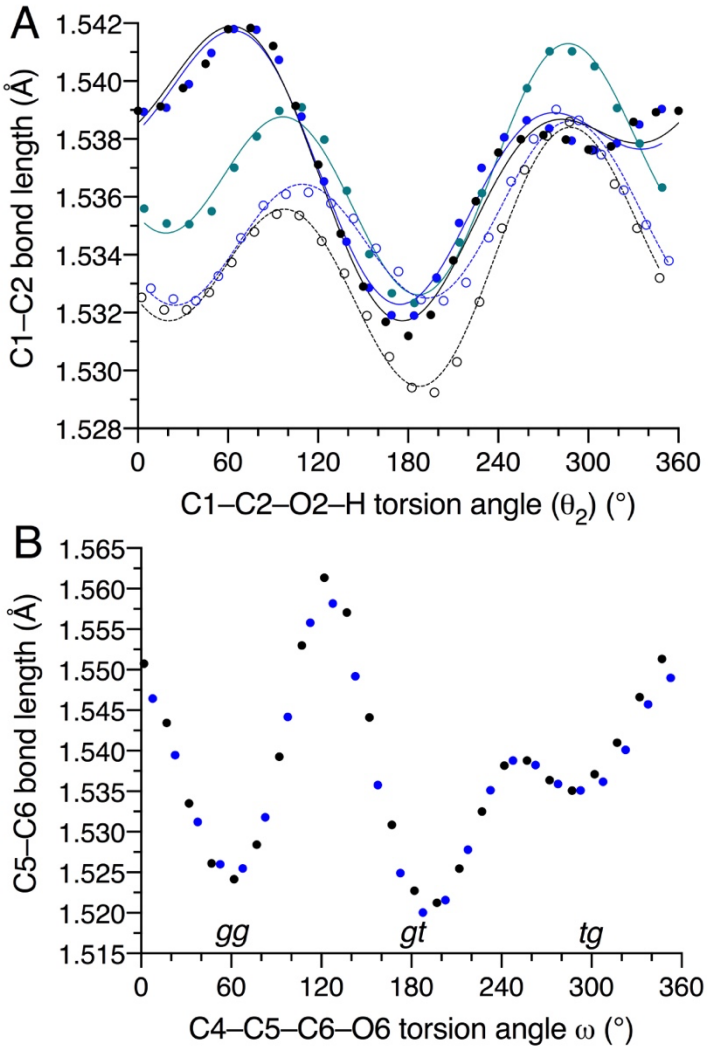

Figure S4. (A) Plot of calculated $r_{C1,C2}$ as a function of the C1–C2–O2–H torsion angle θ_2. Black filled, **1**^{c}. Black open, **2**^{c}. Blue filled, **3**^{c}. Blue open, **4**^{c}. Green filled, **5**^{c}. (B) Plots of $r_{C5,C6}$ as a function of the C4–C5–C6–O6 torsion angle ω. Black filled, **1**^{c}. Blue filled, **2**^{c}. The three staggered rotamers *gg*, *gt* and *tg* are shown associated with their corresponding values of ω.

Table S1. Fitting Statistics from Solid-state ^{13}C NMR Measurements of $^{1}J_{CC}$ values in Crystalline **1**^{1,2}, **1**^{5,6}, **2**^{1,2}, **2**^{5,6}, **3**^{1,2}, **4**^{1,2}, and **5**^{1,2}.

compound	$^{1}J_{CC}$	detected spin	*J*-coupling (Hz)	standard error (Hz)	R^2	average (STDEV) (Hz)
α-GlcOMe (**1**^{1,2})	$^{1}J_{C1,C2}$	C1	48.07	0.10	0.986	48.00 (0.08)
			47.97	0.10	0.988	
			47.97	0.11	0.985	
		C2	48.10	0.11	0.985	
			47.85	0.10	0.987	
			48.03	0.10	0.986	
β-GlcOMe (**2**^{1,2})	$^{1}J_{C1,C2}$	C1	48.57	0.09	0.989	48.57 (0.09)
			48.48	0.09	0.988	
			48.66	0.09	0.989	
		C2	48.64	0.09	0.990	
			48.42	0.10	0.987	
			48.63	0.10	0.987	
α-GalOMe (**3**^{1,2})	$^{1}J_{C1,C2}$	C1	48.74	0.10	0.985	48.82 (0.09)
			49.01	0.11	0.983	
			48.84	0.11	0.983	
		C2	48.80	0.10	0.986	
			48.76	0.10	0.988	
			48.74	0.10	0.988	
β-GalOMe (**4**^{1,2})	$^{1}J_{C1,C2}$	C1	49.12	0.09	0.988	49.07 (0.09)
			49.08	0.09	0.990	
			48.91	0.09	0.989	
		C2	49.05	0.02	0.991	
			49.20	0.09	0.988	
			49.04	0.08	0.992	
α-ManOMe (**5**^{1,2})	$^{1}J_{C1,C2}$	C1	49.78	0.14	0.970	49.42 (0.27)
			49.48	0.14	0.972	
			48.98	0.12	0.979	
		C2	49.70	0.14	0.972	
			49.35	0.14	0.974	
			49.24	0.12	0.981	
α-GlcOMe (**1**^{5,6})	$^{1}J_{C5,C6}$	C5	43.36	0.11	0.993	43.16 (0.12)
			43.10	0.10	0.994	
			43.18	0.10	0.994	
		C6	43.21	0.11	0.992	
			43.45	0.11	0.992	
			43.21	0.11	0.992	
β-GlcOMe (**2**^{5,6})	$^{1}J_{C5,C6}$	C5	44.95	0.11	0.990	44.82 (0.11)
			44.90	0.10	0.991	
			44.93	0.10	0.991	
		C6	44.68	0.10	0.993	
			44.73	0.11	0.990	
			44.73	0.10	0.992	

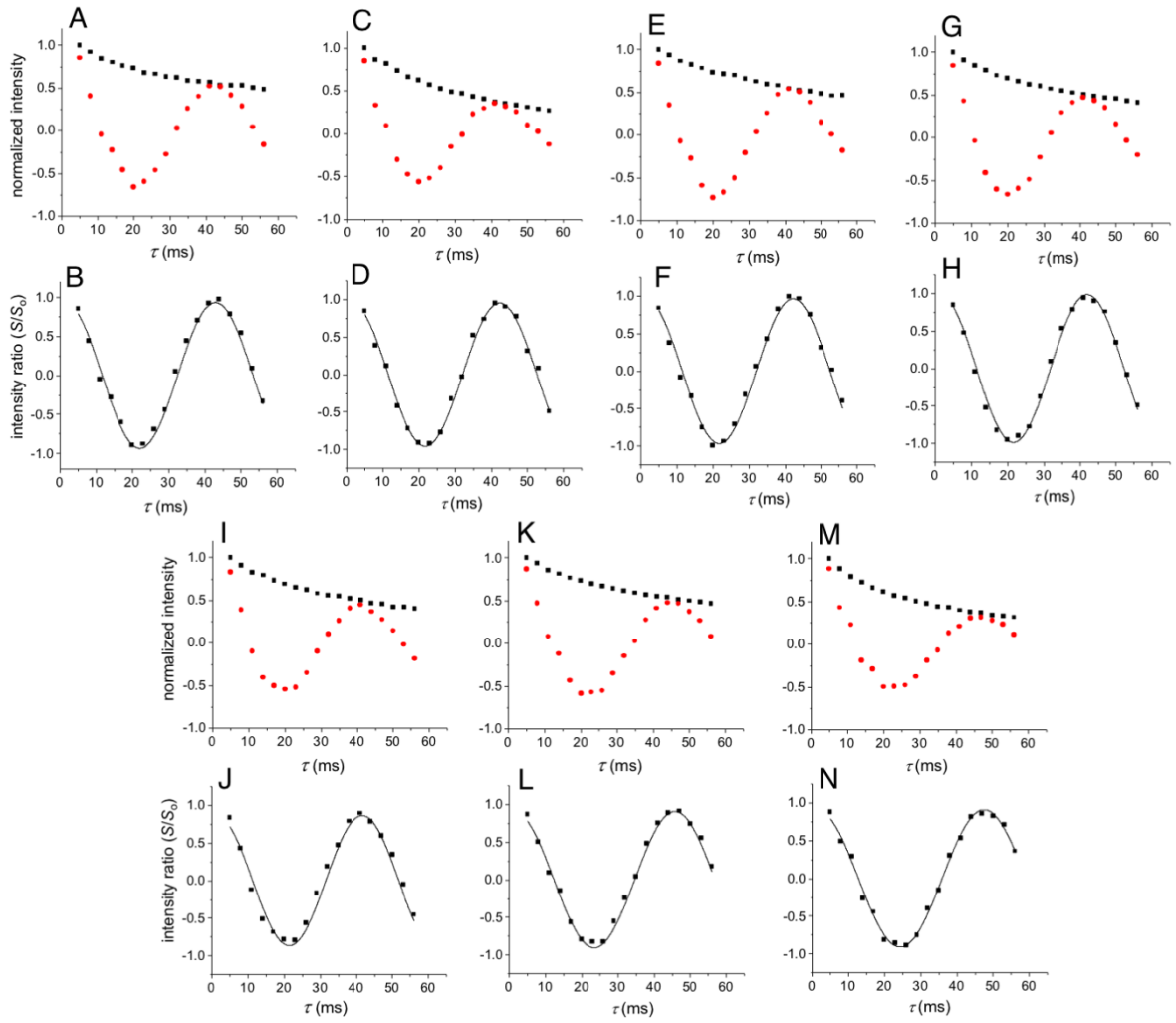

Figure S5. Plots of S/S_o vs τ to determine $^1J_{C1,C2}$ or $^1J_{C5,C6}$ in $\mathbf{1}^{1,2}$ (A and B), $\mathbf{2}^{1,2}$ (C and D), $\mathbf{3}^{1,2}$ (E and F), $\mathbf{4}^{1,2}$ (G and H), $\mathbf{5}^{1,2}$ (I and J), $\mathbf{1}^{5,6}$ (K and L) and $\mathbf{2}^{5,6}$ (M and N). Normalized intensities of the *J*-modulated echo signals (S; red) and the reference echo signals (S_o; black) are plotted against the total echo interval, τ, in A, C, E, G, I, K and M. Intensity ratios, (S/S_o), are plotted against τ in B, D, F, H, J, L and N. The solid black curves represent the best fits to the equation given in references 61 and 62 of the main text. All experiments were run in triplicate, and only one representative signal in the ^{13}C NMR spectra (Figure S3) is shown for each compound.

Discussion of Equation [1] For *J*-Coupling Equation Parameterization

The generalized form of the Karplus-like equation that was used to parameterize the dependence of *J*-couplings on a specific torsion angle was first described by Pachler (K. G. R. Pachler, Extended Hückel Theory MO Calculations of Proton-Proton Coupling Constants–II: The Effect of Substituents on Vicinal Couplings in Monosubstituted Ethanes, *Tetrahedron* 1971, ***27***, 187–199). He proposed the use of this trigonometric function to account for asymmetry in the Karplus curve caused by substitution of a hydrogen atom in the coupling pathway. We adopted this trigonometric polynomial form because it provides the best parameterization to the DFT data with the smallest number of terms. This form of the equation is also amenable to simple integration which allowed us to develop the *MA'AT* equation for modeling torsional populations.

Additional DFT Calculations

In addition to the hydrogen atom optimization discussed in the main text, three additional sets of hydrogen atom optimizations were conducted. These calculations were performed to evaluate the effects of the initial geometry and hydrogen bonding on the optimization. In the first set of calculations (Set 3b), the optimizations were conducted as described in the main text except the input Cartesian coordinates were obtained from HAR structures, as described in the Experimental section and used for calculating $^1J_{CC}$ values in Set 2. The two remaining sets of calculations aimed to examine the effects of hydrogen bonding on optimization. In these calculations (Sets 3c and 3d), methanol molecules surrounding a single saccharide molecule were included to mimic the hydrogen bonding observed in the crystal (Set 1) and the refined (Set 2) structures, respectively. *J*-Couplings were calculated in each optimized structure as described in the main text. For Sets 3c (from X-ray) and 3d (from HAR), the hydrogen bonding was removed before calculating the $^1J_{CC}$ values. For Sets 3e (from X-ray) and 3f (from HAR) the hydrogen bonding was retained for the calculations of the $^1J_{CC}$ values. Sets 3c and 3e have identical geometries for the *J*-coupling calculations except that Set 3e includes the hydrogen bonding. The same applies to Sets 3d and 3f. The calculated $^1J_{CC}$ values are shown in Table S2.

Table S2. Calculated $^1J_{CC}$ Values (In Hz) in $\mathbf{1}^{1,2}$–$\mathbf{5}^{1,2}$, $\mathbf{1}^{5,6}$ and $\mathbf{2}^{5,6}$ Obtained from Different DFT Geometry Optimization and *J*-Coupling Calculations

Input geometry	**X-ray**			**HAR**		
Packing included in geometry optimization	no	yes	yes	no	yes	yes
Packing included in *J*-coupling calculation	no	no	yes	no	no	yes
	Set 3	**Set 3b**	**Set 3c**	**Set 3d**	**Set 3e**	**Set 3f**
$\mathbf{1}^{1,2}$ (αGlc)	49.3	49.2	49.4	48.6	48.9	49.0
$\mathbf{2}^{1,2}$ (βGlc)	51.0	51.3	51.0	51.1	51.3	51.0
$\mathbf{3}^{1,2}$ (αGal)	50.5	50.4	50.4	50.4	50.3	50.3
$\mathbf{4}^{1,2}$ (βGal)	50.8	51.4	51.0	50.7	51.5	51.1
$\mathbf{5}^{1,2}$ (αMan)	52.2	52.8	51.6	51.9	52.5	51.3
$\mathbf{1}^{5,6}$ (αGlc)	45.7	45.6	46.1	45.9	46.0	46.5
$\mathbf{2}^{5,6}$ (βGlc)	44.3	44.3	43.8	44.1	44.5	44.1

In general, different starting structures and/or including hydrogen bonding during geometry optimizations and/or in the $^1J_{CC}$ calculations had little effect on the calculated $^1J_{CC}$ values. In all cases but **1**, including hydrogen bonding in the *J*-coupling calculations lowered the calculated $^1J_{CC}$ values by 0.0–1.2 Hz (Set 3b – Set 3c, and Set 3e – Set 3f), with an average difference of 0.24 Hz. Changing the input coordinates for geometry optimization resulted in minor changes in the calculated $^1J_{CC}$ values (–0.2–0.7 Hz; Set 3 – Set 3d) with an average difference of 0.16 Hz. The average standard deviation of all methods was 0.28 Hz, indicating that neither the starting geometry nor hydrogen bonding has a significant impact on calculated $^1J_{CC}$ values.

Torsional Dependencies of $^1J_{C5,C6}$ Values

$^1J_{C5,C6}$ values in aldohexopyranosyl rings depend strongly on both the ω (C4–C5–C6–O6) and θ_6 (C5–C6–O6–H) torsion angles. As discussed in prior work on $^1J_{CC}$ in vicinal diol fragments (*J. Am. Chem. Soc.* 2004, ***126***, 15668–15685), it is possible to derive parameterized equations that include both angles and describe an hypersurface. However, due to the complexity of parameterizing a surface, the present work examined only the dependence on ω, since θ_6 is fixed at a known value in crystalline samples.

However, for the sake of completeness, the hypersurface was determined for **2** for comparison to results reported in the prior 2004 *JACS* study. In these DFT calculations, both ω and θ_6 in **2** were rotated in 15° increments through 360°, yielding 576 optimized structures. The geometry optimizations were conducted as described in the main text at the B3LYP/6-31G* level of theory, and $^1J_{C5,C6}$ values were calculated, again as described in the main text. The resulting hypersurface is shown in Figure S6.

Figure S6. Hypersurface showing the dual dependencies of $^1J_{C5,C6}$ in **2** on the ω (C4–C5–C6–O6) and θ_6 (C5–C6–O6–H) torsion angles. Maximal coupling is observed in the *tg* rotamer (ω = 300°; O5 and O6 *anti*) when O6H is *anti* to C5 (θ_6=180°).

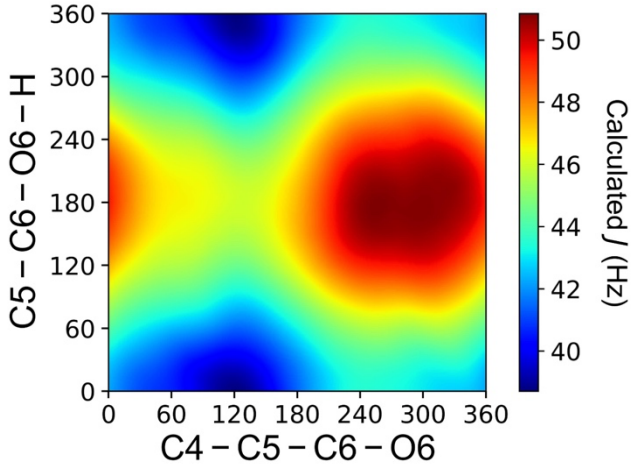

X- and *Y*-axis 2D projections of the hypersurface are shown in Figure S7. These plots show the extent to which $^1J_{C5,C6}$ is affected by ω and θ_6. Coupling is maximal when O5 and O6 are *anti* (ω = 300°) (Plot A) and when C5 and O6H are *anti* (θ_6 = 180°)(Plot B), a result consistent with those of prior studies of $^1J_{CC}$ in vicinal diols (see *JACS* reference above). The plane of symmetry of the hypersurface should allow an equation to be parameterized for $^1J_{C5,C6}$ containing two variables, ω and θ_6.

Figure S7. Plots of *x*- and *y*-axis projections of the data shown in Figure S6. (A) Plot of $^1J_{C5,C6}$ *vs* ω, showing data scatter at discrete values of ω caused by θ_6. (B) Plot of $^1J_{C5,C6}$ *vs* θ_6, showing data scatter at discrete values of θ_6 caused by ω.

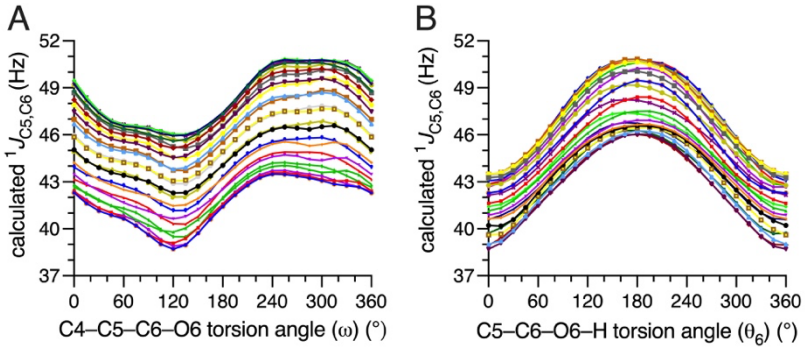

Representative Cartesian Coordinates for DFT Structures 1[c]–5[c]

Structure **1**[c]

O	1.867	6.623	8.371
O	3.861	4.968	7.287
H	3.18	5.006	6.785
O	2.826	2.567	8.416
H	2.216	2.077	8.082
O	0.804	2.979	10.537
H	0.98	2.178	10.296
O	2.626	6.128	10.542
O	0.604	6.391	12.689
H	1.147	7.004	12.86
C	2.958	6.227	9.162
H	3.647	6.887	9.138
C	3.427	4.874	8.633
H	4.197	4.595	9.164
C	2.329	3.837	8.836
H	1.519	4.068	8.297
C	1.948	3.794	10.313
H	2.725	3.457	10.787
C	1.57	5.191	10.809
H	0.77	5.506	10.353
C	1.315	5.219	12.303
H	0.734	4.479	12.52
H	2.133	5.152	12.784
C	1.372	7.919	8.701
H	0.713	8.126	8.001
H	2.096	8.587	8.73
H	0.964	7.958	9.599

Structure **2**[c]

O	4.724	5.253	19.945
O	7.17	5.826	21.238
H	6.642	6.083	21.816
O	8.877	3.607	21.554
H	9.551	3.13	21.406
O	8.857	1.766	19.28
H	9.133	1.183	19.828
O	5.512	3.226	19.255
O	5.265	1.21	17.159
H	4.599	1.719	17.315
C	5.876	4.575	19.601
H	6.326	4.974	18.818
C	6.806	4.515	20.806
H	6.348	4.034	21.522
C	8.056	3.752	20.399

H	8.552	4.291	19.706
C	7.692	2.379	19.83
H	7.34	1.859	20.546
C	6.637	2.495	18.732
H	6.995	2.968	17.961
C	6.113	1.14	18.294
H	6.855	0.588	18.043
H	5.635	0.735	19.053
C	3.893	5.541	18.803
H	3.078	5.995	19.146
H	3.6	4.724	18.384
H	4.394	6.098	18.142

Structure **3**[c]

O	3.889	1.132	8.947
O	5.432	0.239	6.951
H	5.501	-0.126	6.201
O	6.659	2.701	6.106
H	7.35	2.796	6.489
O	4.264	4.175	5.715
H	4.744	4.642	5.366
O	2.789	2.681	7.591
O	1.65	4.875	8.958
H	1.947	4.798	9.705
C	3.472	1.432	7.643
H	2.839	0.793	7.338
C	4.712	1.448	6.748
H	4.414	1.542	5.829
C	5.592	2.652	7.066
H	5.989	2.558	7.97
C	4.777	3.945	7.023
H	5.33	4.665	7.332
C	3.605	3.809	7.986
H	3.932	3.656	8.881
C	2.702	5.024	8.013
H	3.254	5.777	8.228
H	2.283	5.147	7.099
C	2.799	0.985	9.869
H	3.156	0.527	10.646
H	2.094	0.46	9.494
H	2.442	1.854	10.098

Structure **4**[c]

O	5.211	4.602	6.392
O	2.714	3.564	7.406
H	2.486	3.6	6.676
O	2.958	1.048	8.735

H	2.826	0.832	7.979
O	5.659	0.481	8.178
H	6.069	-0.093	8.587
O	6.343	3.276	7.849
O	8.656	3.216	9.503
H	9.135	3.269	8.801
C	5.103	3.933	7.61
H	4.919	4.543	8.311
C	3.974	2.91	7.515
H	4.139	2.377	6.752
C	3.944	2.068	8.789
H	3.714	2.649	9.506
C	5.315	1.497	9.127
H	5.259	1.095	10.008
C	6.34	2.629	9.138
H	6.093	3.32	9.82
C	7.743	2.128	9.412
H	7.73	1.664	10.251
H	8.015	1.486	8.698
C	5.965	5.815	6.497
H	5.915	6.266	5.646
H	6.88	5.638	6.767
H	5.575	6.394	7.171

Structure **5**[c]

O	5.211	4.602	6.392
O	2.714	3.564	7.406
H	2.486	3.6	6.676
O	2.958	1.048	8.735
H	2.826	0.832	7.979
O	5.659	0.481	8.178
H	6.069	-0.093	8.587
O	6.343	3.276	7.849
O	8.656	3.216	9.503
H	9.135	3.269	8.801
C	5.103	3.933	7.61
H	4.919	4.543	8.311
C	3.974	2.91	7.515
H	4.139	2.377	6.752
C	3.944	2.068	8.789
H	3.714	2.649	9.506
C	5.315	1.497	9.127
H	5.259	1.095	10.008
C	6.34	2.629	9.138
H	6.093	3.32	9.82
C	7.743	2.128	9.412
H	7.73	1.664	10.251
H	8.015	1.486	8.698

C	5.965	5.815	6.497
H	5.915	6.266	5.646
H	6.88	5.638	6.767
H	5.575	6.394	7.171

Complete Reference 50

M. J. Frisch, G. W. Trucks, H. B. Schlegel, G. E. Scuseria, M. A. Robb, J. R. Cheeseman, G. Scalmani, V. Barone, G. A. Petersson, H. Nakatsuji, X. Li, M. Caricato, A. V. Marenich, J. Bloino, B. G. Janesko, R. Gomperts, B. Mennucci, H. P. Hratchian, J. V. Ortiz, A. F. Izmaylov, J. L. Sonnenberg, D. Williams-Young, F. Ding, F. Lipparini, F. Egidi, J. Goings, B. Peng, A. Petrone, T. Henderson, D. Ranasinghe, V. G. Zakrzewski, J. Gao, N. Rega, G. Zheng, W. Liang, M. Hada, M. Ehara, K. Toyota, R. Fukuda, J. Hasegawa, M. Ishida, T. Nakajima, Y. Honda, O. Kitao, H. Nakai, T. Vreven, K. Throssell, J. A. Montgomery, Jr., J. E. Peralta, F. Ogliaro, M. J. Bearpark, J. J. Heyd, E. N. Brothers, K. N. Kudin, V. N. Staroverov, T. A. Keith, R. Kobayashi, J. Normand, K. Raghavachari, A. P. Rendell, J. C. Burant, S. S. Iyengar, J. Tomasi, M. Cossi, J. M. Millam, M. Klene, C. Adamo, R. Cammi, J. W. Ochterski, R. L. Martin, K. Morokuma, O. Farkas, J. B. Foresman, and D. J. Fox, *Gaussian*16, Revision C.01, Gaussian, Inc., Wallingford CT, 2019.

References

1. M. C. Pirrung, *The Synthetic Organic Chemist's Companion;* Wiley & Sons, Inc.: Hoboken, NJ, 2007; Appendix 3: Recipes for TLC Stains
2. P. W. Austin, F. E. Hardy, J. G. Buchanan and J. Baddiley, *J. Chem. Soc.*, 1963, 5350–5353.
3. A. Watson, S. Hackbusch and A. H. Franz, *Carbohydr. Res.* 2019, **473**, 18–35.
4. S. Wang, X. Wen, A. L. DeVries, Y. Bagdagulyan, A. Morita, J. A. Golen, J. G. Duman and A. L. Rheingold, *J. Am. Chem. Soc.* 2014, **136,** 8973–8981.
5. Z. Shi, L. Sun and C. Li, *J. Agric. Food Chem.*, 2014, **62**, 3287–3292.
6. O. Moradei, C. du Mortier, A. Fernandez Cirelli and J. Thiem, *J. Carbohydr. Chem.*, 1995, **14**, 525–532.
7. S. van der Vorm, T. Hansen, H. S. Overkleeft, G. A. van der Marel and J. D. C. Codee, *R. Soc. Chem.,* 2017, **8**, 1867–1875.
8. H. M. Berman and S. H. Kim, *Acta Cryst.*, 1968, **B24**, 897–904.
9. G. A. Jeffrey, R. K. McMullan and S. Takagi, *Acta Cryst.*, 1977, **B33**, 728–737.
10. G. A. Jeffrey and S. Takagi, *Acta Cryst.*, 1977, **B33**, 738–742.
11. T. Turney, Q. Pan, W. Zhang, A. G. Oliver and A. S. Serianni, *Acta Cryst. C*, 2019, **75**, 161–167.

12. B. M. Gatehouse and B. J. Poppleton, *Acta Cryst.*, 1971, **B27**, 654–660.

13. S. Takagi and G. A. Jeffrey, *Acta Cryst.*, 1979, **B35**, 902–906.

14. S. Takagi and G. A. Jeffrey, *Acta Cryst.,* 1978, **B34**, 2006–2010.

15. B. M. Gatehouse and B. J. Poppleton, *Acta Cryst.*, 1970, **B26**, 1761–1765.

16. B. Bose-Basu, T. Klepach, G. Bondo, P. B. Bondo, W. Zhang, I. Carmichael and A. S. Serianni, *J. Org. Chem.*, 2007, **72**, 7511–7522.

17. C. Thibaudeau, R. Stenutz, B. Hertz, T. Klepach, S. Zhao, Q. Wu, I. Carmichael and A. S. Serianni, *J. Am. Chem. Soc.*, 2004, **126**, 15668–15685.